Available online at www.sciencedirect.com

ScienceDirect

Mendeleev Commun., 2017, **27**, 531–534

Mendeleev Communications

One-pot sol-gel synthesis of porous silica glass with gold nanoparticles

Andriy P. Budnyk,*[a,b] Svetlana O. Cherkasova[a] and Alessandro Damin[b]

[a] *International Research Center 'Smart Materials', Southern Federal University, 344090 Rostov-on-Don, Russian Federation. E-mail: abudnik@sfedu.ru*

[b] *Department of Chemistry, University of Turin, 10125 Turin, Italy*

DOI: 10.1016/j.mencom.2017.09.035

A new simple one-pot synthesis of mesoporous silica monolith containing gold nanoparticles is proposed, offering a convenient model for the spectroscopic studies of particle-related phenomena.

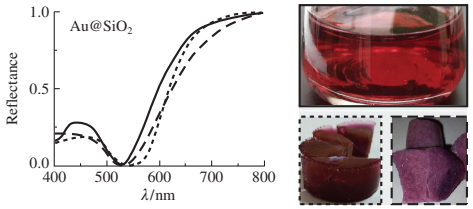

The fascinating properties of nanosized noble metals, including silver and gold, both sharing similar plasmonic optical properties, synthesis procedures and areas of application,[1] are of considerable current interest. The supported gold and silver nanoparticles (NPs) are known as amplifiers for the molecular vibrations of probes in surface-enhanced Raman spectroscopy (SERS).[2] Among the examples of such systems, silver NPs formed by ultrasonic rain deposition on glass and then covered by a polymer,[3(a)] silver NPs on graphene oxide produced by aerosol spray pyrolysis[3(b)] gold NPs on mesoporous cellulose obtained by combining metal-vapor synthesis with sol-gel technology and freeze-drying procedures,[3(c)] gold NPs on activated carbon prepared by impregnation and reduction in hydrogen flow,[3(d)] and gold NPs decorating DNA scaffolds synthesized by the sodium borohydride reduction of gold chloride[3(e)] should be mentioned.

The Turkevich method[4] of gold or silver salt reduction by citrate in aqueous solution is widely used to produce stable colloidal solutions of metal NPs. The simplicity and reproducibility of the method inspired further efforts for better control over the shape and size distribution of NPs.[5] The resulting solution represents a model system composed of metal nano-objects homogeneously dispersed in an optically transparent medium. Changes in the size, shape, and aggregation state of gold NPs influence the peak position, width and profile of a surface plasmon resonance (SPR) absorption band in the optical spectrum.[6] However, the instability of colloids encourages the development of easy-to-obtain and stable model systems for the optical spectroscopy of metal NPs.[7]

Glass is a natural choice for an optically transparent material with chemical inertness and good stability over time. Gold-containing glass can be prepared by melting, high-pressure processing, and sol-gel synthesis.[8] Metal NPs can be introduced into the volume of pre-formed porous glass by soaking it in the solutions of colloidal gold or gold salts with consecutive thermal reduction.[9] Another way is the dispersion of a gold precursor (or pre-formed NPs) in a mixture of reagents (so-called one-pot synthesis).[10] To control the size distribution of gold NPs, capping agents containing thiol or amine groups are used.[11] The introduction of additional elements may poison the surface of gold NPs limiting the possibility to study surface-related phenomena in SERS.[12]

Our protocol for the sol-gel synthesis was already employed for the production of titanium- and chromium-doped mesoporous silica monoliths.[13] The silica matrix was found preserving its porosity and surface area under thermal treatment in a range of 550–750 °C.[13(c)] At the doping level under 1 wt%, the final products demonstrated good catalytic activity due to isolated metal sites homogeneously distributed over the silica surface. A higher loading of guest metal precursor led to the formation of metal oxide NPs embedded in a silica network. The conversion of gold chlorides into gold oxides is unlikely to occur in this process.[9] Instead, even tiny amounts of loaded gold form metal NPs, which despite being scarcely distributed provide strong coloration for the material due to a high efficiency of light scattering.[14]

This communication focuses on the optical properties of porous glass monoliths containing gold NPs, whose morphological properties will be compared to those of bare silica glass, while the plasmonic ones will be contrasted with those of colloidal gold solution. Inspired by the simplicity of the Turkevich method, we have followed his recipe with slight modifications to obtain stable colloids of gold NPs.† For the acid-catalyzed sol-gel synthesis, we have chosen hydrochloric acid instead of nitric acid, which was adopted previously.[13] The use of HCl reduces the gelation time of TEOS in ethanol, defines the rate and extent of the hydrolysis of TEOS, and affects the pore morphology and surface area to provide a material of high optical quality.[15] An adoption of a simple one-pot sol-gel synthesis (with the

† The reagents were commercial tetraethoxysilane [TEOS, $(EtO)_4Si$, 99%], ethanol (90%), hydrochloric acid (diluted 1 : 10 with H_2O), sodium tetrachloroaurate(III) dihydrate ($AuCl_4Na{\cdot}2H_2O$, 99%), sodium citrate ($C_6H_7NaO_7$, 99%); ultra-pure water (18 MΩ) was obtained on a SimplicityUV system. The reagents in the molar ratio $(EtO)_4Si : H_2O : EtOH = 1 : 10 : 6$ were mixed with stirring. The pH 2 was adjusted by the dropwise addition of dilute HCl, allowing hydrolysis to occur. To obtain gold-containing samples, the gold salt was added at this stage in quantity of Au 1 wt% to dry SiO_2 (for Au@SiO_2 sample), and then sodium citrate in the ratio Au : Cit = 1:6 (for T_Au@SiO_2 sample) was added. The mixture was stirred for 1 h. Next, it was poured into a plastic vessel and sealed. The thermal treatment included gel formation at 60 °C for two days, gel aging at 80 °C for five days and gel drying (vessel was pin-holed) for seven days with slowly heating to 120 °C. The obtained xerogel was stabilized at 600 °C for 1 h, which was preceded by slow heating at a rate of 1 K min^{-1}.

loading of 3 wt% Au to SiO_2) resulted in an intensely colored $Au@SiO_2$ mesoporous monolith with excess gold forming microcrystals.[16] Here, we use this method to produce $Au@SiO_2$ monolith with 1 wt% Au. Then, we combined it with a citrate-reduction method to form gold NPs exhibiting optical properties resembling those of colloidal solution after Turkevitch. We also noticed that the direct addition of pre-formed gold NPs into the reagent mixture led to their precipitation at the bottom of the gel (formed under the adopted sol-gel synthesis protocol). The synthesized samples† are marked as follows: SiO_2 for pure silica monolith, $Au@SiO_2$ for silica monolith with gold NPs prepared by the one-pot method, $T\_Au@SiO_2$ for silica monolith with gold NPs prepared by a combination of one-pot protocol with a citrate-reduction method, and $Au@H_2O$ for the gold colloidal solution. All gold-containing samples exhibit a characteristic red color; $Au@SiO_2$ was transparent and $T\_Au@SiO_2$ was opaque. The monoliths are easy-to-handle: it is possible to cut mechanically a slice of desired thickness to tune the level of adsorption; alternatively, they can be grounded into powder by a pestle and mortar.

The porosity of the glass monoliths was confirmed by nitrogen sorption measurements.‡ The adsorption isotherms can be classified as type IV according to the IUPAC classification.[17] The pore size was about 4–5 nm (Figure 1), confirming the attribution. The hysteresis loop of H4 type[17] appears for all the samples at relative pressures over $p/p_0 = 0.5$. The step caused by the release of nitrogen, which has been liquified in the pores during the adsorption branch run at higher relative pressures. The overall

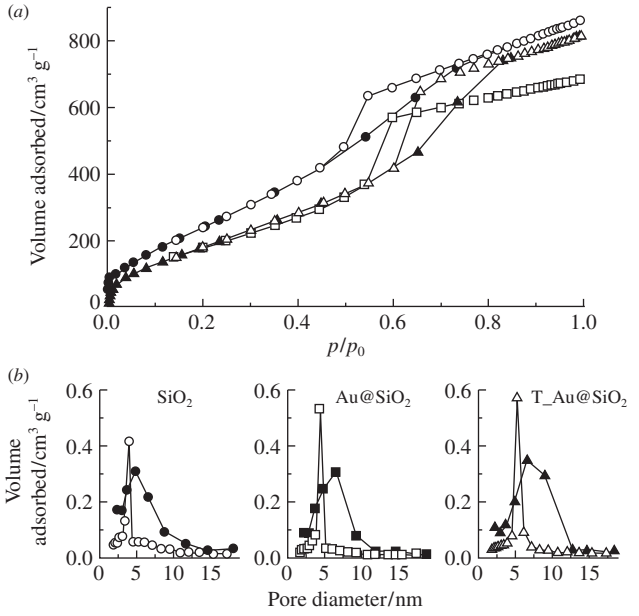

Figure 1 (*a*) N_2 sorption isotherm and (*b*) respective BJH pore size distributions measured on (●, ○) SiO_2, (■, □) $Au@SiO_2$ and (▲, △) $T\_Au@SiO_2$. Solid symbols correspond to the adsorption branch of an isotherm, and empty ones refer to the desorption branch.

‡ The N_2 adsorption/desorption isotherms at –196 °C were obtained using an ASAP 2020 station (Micromeritics). Specific surface area (SSA) values were calculated by the instrument software on the basis of Brunauer–Emmett–Teller (BET) theory, and pore diameter was evaluated by Barrett–Joyner–Halenda (BJH) analysis. The XRD patterns were collected on a Phaser D2 Powder diffractometer (Bruker) using CuKα radiation. The optical spectroscopy measurements were performed with a UV-2600 spectrophotometer (Shimadzu). The IR and Raman spectra were recorded on a FSM 1202 FTIR spectrometer (Infraspec) and an InVia Renishaw microscope with 785 nm excitation laser, respectively. The SERS spectrum was collected by letting 10 μl of 10 mmol aqueous pyridine solution to vaporize inside a sealed Suprasil UV-VIS cell with the sample.

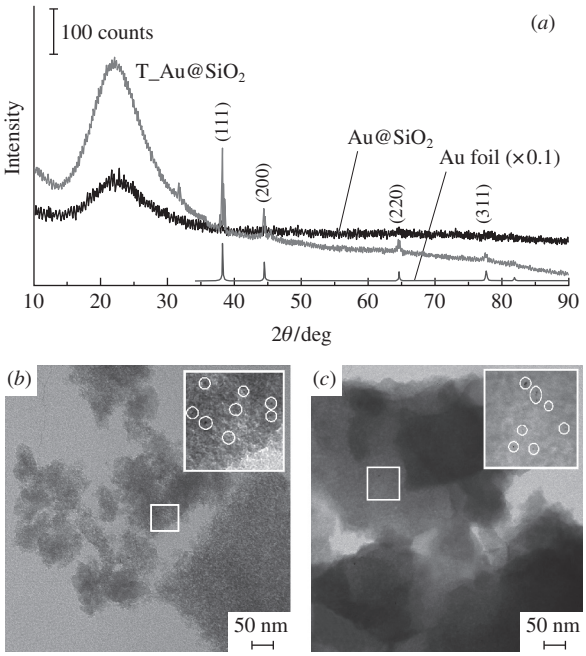

Figure 2 (*a*) XRD patterns and (*b*), (*c*) TEM images for $Au@SiO_2$ and $T\_Au@SiO_2$ samples, respectively.

porosity was estimated at ~50% on a density and weight basis. The difference in gas uptake by pure monolith and both composites is about 150 $cm^3\ g^{-1}$, which reflected in a noticeable deviation in SSA values. The SiO_2 sample has SSA of 910 $m^2\ g^{-1}$ by BET, while both $Au@SiO_2$ and $T\_Au@SiO_2$ exhibit smaller values of 640 and 681 $m^2\ g^{-1}$, respectively. The reduction of SSA by a factor 0.7 in gold-containing samples could be attributed to gold NPs grown in the pores and partially blocking the internal spaces from an access of nitrogen.[18]

Silica glass is an amorphous material whose SiO_4 tetrahedra are randomly oriented due to the flexibility of Si–O–Si bonds. They may arrange into few-member chains without establishing a long order, as evidenced by a halo in the XRD profiles of monoliths [Figure 2(*a*)]. The weak narrow reflexes of gold-containing samples correspond to a cubic face-centered phase (represented by gold foil), indicating the formation of metal crystallites. They can be inevitably produced already at the gelation stage due to gold salt partial reduction in a water–alcohol mixture on the walls of silica.[19] The representative TEM images of $Au@SiO_2$ and $T\_Au@SiO_2$ samples [Figure 2(*b*),(*c*)] evidence the formation of gold NPs smaller than 10 nm (both isolated and arranged in small groups being scarcely distributed across the SiO_2 matrix volume).

The optical spectra of $Au@H_2O$, $Au@SiO_2$ and $T\_Au@SiO_2$ (Figure 3) around the gold SPR for the sake of clarity were measured in both transmittance and reflectance modes,‡ giving a more complete picture of optical properties than those typically published.[2–6,8–11] All of them exhibit similar profiles of a characteristic symmetrical plasmonic band at 524–547 nm. The SPR broadening of noble NPs is typically influenced by input from their size and shape inhomogeneities or roughly round small (~2 nm) particles and their interaction with a surrounding dielectric medium.[5,10] The maximum of $Au@H_2O$ stays at 524 nm, a characteristic position of gold colloidal solution.[5] The SPR band of $Au@SiO_2$ appears to be red-shifted to 547 nm. In published reports on similar $Au@SiO_2$ systems, this value corresponds to Au NPs of 4–6 nm,[8,9] which seems comparable with the particles observed by TEM [Figure 2(*b*),(*c*)]. The maximum of $T\_Au@SiO_2$ occupies an intermediate position at 530 nm, suggesting the presence of slightly larger Au NPs (not totally excluding the effect of SiO_2 matrix). Summarizing, the observed

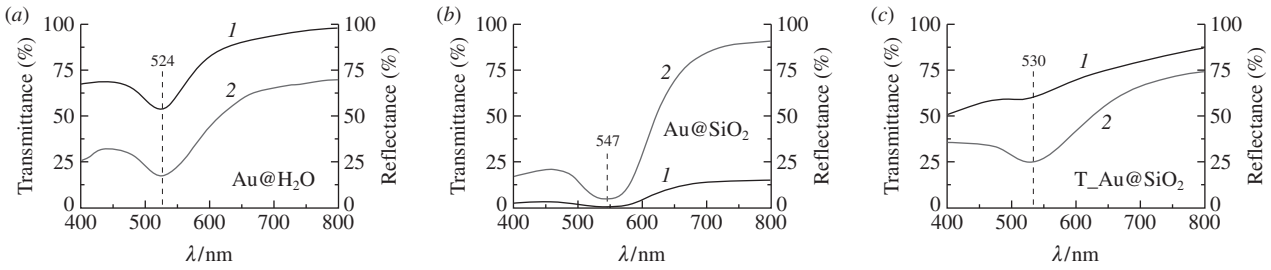

Figure 3 UV-VIS (*1*) transmittance and (*2*) reflectance spectra of (*a*) $Au@H_2O$, (*b*) $Au@SiO_2$ and (*c*) $T\_Au@SiO_2$ samples.

similarity of the optical properties proves that a solid system optically equivalent to colloidal gold solution has been obtained. Gold clusters in a glass medium are known to preserve the extended stability.[8(*a*)]

The growth mechanism of gold NPs under citrate reduction in aqueous solution was already envisaged.[4,5] The generation of the initial nuclei is described by (i) all Au^{3+} getting reduced into Au^0 and then aggregate into nuclei and (ii) unreduced metal species arranging a complex prior to full reduction.[20(*a*)] The latter describes the color changes occurring in solution due to the initial formation of chain-like Au nanowires followed by fragmentation into spherical particles.[20(*b*)] The nucleation curve has a shape characteristic of an autocatalytic reaction.[4]

The dominant growth mechanism for Au NPs in the test $Au@SiO_2$ composites is the thermally induced reduction of Au^{III}, which was already observed in similar systems. For instance, Shi *et al.*[9] performed a 1–16 h heating at 700 °C of the mesoporous SiO_2 being soaked in a gold precursor and found that a plasmon peak shifts from 548 to 523 nm with treatment time, which corresponds to Au NPs size growth from 4 to 15 nm. Kan *et al.*[19] reported that the annealing of mesoporous SiO_2 soaked in a gold precursor up to 300 °C results in the formation of Au nanowires inside the pores of silica. The optical properties of such a composite are tunable by the subsequent annealing at different temperatures.

We followed the thermal annealing of $Au@SiO_2$ using UV-VIS spectroscopy (Figure 4). The first spectrum, taken at 25 °C from the yellow reagent mixture, is identical to that of an aqueous chloroaurate solution.[19] The next curve (at 120 °C) coming from a dried yellow-orange xerogel contains an absorption band at 514 nm, which suggests the formation of single Au NPs *via* the above mechanism. Three successive spectra (at 200, 400 and 600 °C) illustrate a blue shift and narrowing of the plasmon band, evidencing the formation of Au NPs, responsible for a red color of the monolith. Unlike $Au@SiO_2$, the $T\_Au@SiO_2$ sample as a xerogel was brownish (a color typical of Au NPs aggregates dispersed in SiO_2).[21] This color cannot be attributed to organic residuals and oxygen deficiency in SiO_2 matrix,[8(*a*)] but it suggests a certain extent of Au^{III} reduction on gelation due to the action of citrate anions. Successive thermal treatment led to the appearance of a plasmon band at 530 nm [Figure 3(*c*)]. The final difference between the optical profiles of $T\_Au@SiO_2$ and $Au@SiO_2$ samples is evidently due to the introduction of citrate. In this regard, the addition of a reducing agent into the reagent mixture would initiate the reduction of Au^{III} precursors before thermal treatment, affecting the optical properties of the final $Au@SiO_2$ composite. A gentle rise of temperature at the mixing stage would be beneficial for reduction efficiency.

Moving towards the spectroscopic applications of $Au@SiO_2$, the vibrational characterization can be completed with complementary IR and Raman spectra presented in Figure 5 for $T\_Au@SiO_2$ sample against SiO_2. The profiles contain SiO_4 tetrahedra vibrations with the participation of surface Si–OH silanol groups and physisorbed water molecules.[12,15] The similarity of the vibrational spectra also confirms that, by following the same preparation protocol for the samples, the additional effects due to the density and refraction index of a SiO_2 matrix,[8(*b*)] [Figure 3(*b*),(*c*)] were minimized.

It is well established for mesoporous glasses that all the pores are interconnected and open to ambient air.[9] Hence, gold NPs grown in pores are in contact with air. Such a situation allows particles to interact with probe molecules. As a test for SERS, we allowed a vapor of aqueous pyridine (10^{-3} M) to interact with pristine SiO_2 and $Au@SiO_2$ sample.[‡] Small quantity of probe results in no appreciable signal from pristine SiO_2 (see Figure 5), while there are clearly observable ring breathing modes of pyridine interacting with surface hydroxyls *via* H-bonding.[21] This evidence of SERS indicates suitability of $Au@SiO_2$ composite

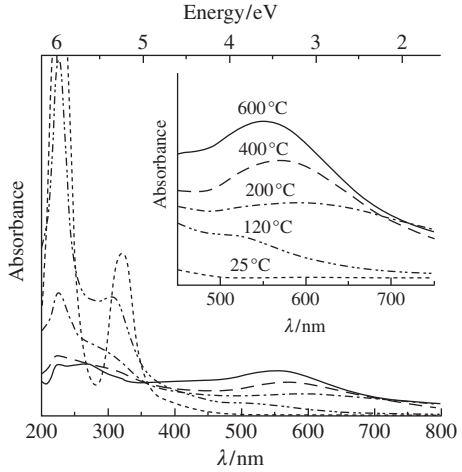

Figure 4 UV-VIS spectra of precursor solution for $Au@SiO_2$ sample (marked as 25 °C), $Au@SiO_2$ xerogel (120 °C) and that annealed at different temperatures (200, 400 and 600 °C). Inset: the magnification of a plasmon peak range.

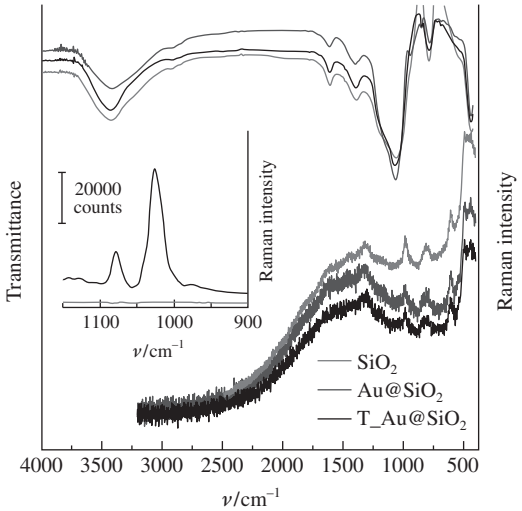

Figure 5 FTIR and Raman spectra of SiO_2 and $Au@SiO_2$ samples. Inset: SERS of pyridine (concentration, 10 mmol dm^{-3}) on $Au@SiO_2$.

to catch a target analyte for possible SERS analysis. An additional commodity is the possibility to clean-up the composite from adsorbed organic molecules by heating it at about 500 °C.

Apart of SERS sensing, the surface plasmon peak can be used for selective optical gas sensing by porous matrices containing functional nanocrystals of metal oxides and gold. Thus, a sol-gel SiO_2 porous film containing NiO and Au NPs capable of hydrogen detection based on a chromatic transition in the plasmon peak was described.[8(c)] Building bridges between the phenomena underlying SPR and advanced physical studies on noble metal NPs like that of ultrafast dynamics of electron–phonon and phonon–phonon relaxation under femtosecond laser pulses were considered.[22] In this regard, the Au@SiO_2 plasmonic composites are very promising materials for ultrafast optical switches and modulators.[8(a)]

In conclusion, the simple sol-gel synthesis allowed us to produce various chemically pure composites, the mesoporous glass monoliths containing homogeneously dispersed gold NPs. The addition of citrate to a one-pot mixture influenced the final optical properties. The key features of the Au@SiO_2 composites are (1) the equivalence of the optical properties of gold NPs in transparent liquid and solid media; (2) the accessibility of Au NPs for interaction with probe molecules, allowing for SERS and optical sensing. The composites are stable and easy-to-operate; they can be used in bulk and powder forms.

This work was supported by the Government of the Russian Federation (agreement no. 14.Y26.31.0001). S.O.Ch. acknowledges the support of Southern Federal University (a student academical mobility grant).

References

1 (*a*) J. Z. Zhang and C. Noguez, *Plasmonics*, 2008, **3**, 127; (*b*) M.-C. Daniel and D. Astruc, *Chem. Rev.*, 2004, **104**, 293.
2 (*a*) B. Sharma, R. R. Frontiera, A.-I. Henry, E. Ringe and R. P. Van Duyne, *Mater. Today*, 2012, **15**, 16; (*b*) A. A. Semenova, A. P. Semenov, E. A. Gudilina, G. T. Sinyukova, N. A. Brazhe, G. V. Maksimov and E. A. Goodilin, *Mendeleev Commun*., 2016, **26**, 177.
3 (*a*) A. V. Sidorov, O. E. Eremina, I. A. Veselova and E. A. Goodilin, *Mendeleev Commun*., 2015, **25**, 460; (*b*) M. O. Volodina, A. Yu. Polyakov, A. V. Sidorov, A. V. Grigorieva, E. A. Eremina, S. V. Savilov and E. A. Goodilin, *Mendeleev Commun*., 2016, **26**, 231; (*c*) A. Yu. Vasil'kov, M. S. Rubina, A. A. Gallyamova, A. V. Naumkin, M. I. Buzina and G. P. Murav'eva, *Mendeleev Commun.*, 2015, **25**, 358; (*d*) G. N. Bondarenko and I. P. Beletskaya, *Mendeleev Commun*., 2015, **25**, 443; (*e*) L. I. Lopatina, E. A. Karpushkin, A. Zinchenko and V. G. Sergeyev, *Mendeleev Commun*., 2016, **26**, 291.
4 J. Turkevich, P. C. Stevenson and J. Hillier, *Discuss. Faraday Soc.*, 1951, **11**, 55.
5 (*a*) G. Frens, *Nat. Phys. Sci.*, 1973, **20**, 241; (*b*) J. Kimling, M. Maier, B. Okenve, V. Kotaidis, H. Ballot and A. Plech, *J. Phys. Chem. B*, 2006, **110**, 15700; (*c*) K. Zabetakis, W. E. Ghann, S. Kumar and M.-C. Daniel, *Gold Bull.*, 2012, **45**, 203.
6 L. M. Liz-Marzán, *Langmuir*, 2006, **22**, 32.
7 G. A. Wurtz, R. J. Pollard and A.V. Zayats, in *Handbook of Nanoscale Optics and Electronics*, ed. G. Wiederrecht, Elsevier, Amsterdam, 2010.
8 (*a*) M. Eichelbaum, K. Rademann, R. Müller, M. Radtke, H. Riesemeier and W. Görner, *Angew. Chem. Int. Ed*., 2005, **44**, 7905; (*b*) M. T. Laranjo, T. B. L. Kist, E. V. Benvenutti, M. R. Gallas and T. M. H. Costa, *J. Nanopart. Res*., 2011, **13**, 4987; (*c*) E. Della Gaspera, D. Buso and A. Martucci, *J. Sol-Gel Sci. Technol*., 2011, **60**, 366.
9 H. Shi, L. Zhang and W. Cai, *Mater. Res. Bull.*, 2000, **35**, 1689.
10 M. C. Ferrara, L. Mirenghi, A. Mevoli and L. Tapfer, *Nanotechnology*, 2008, **19**, 365706.
11 J. D. S. Newman and G. J. Blanchard, *Langmuir*, 2006, **22**, 5882.
12 A. Damin, S. Usseglio, G. Agostini, S. Bordiga and A. Zecchina, *J. Phys. Chem. C*, 2008, **112**, 4932.
13 (*a*) A. Budnyk, A. Damin, S. Bordiga and A. Zecchina, *J. Phys. Chem. C*, 2012, **116**, 10064; (*b*) A. Budnyk, A. Damin, C. Barzan, E. Groppo, C. Lamberti, S. Bordiga and A. Zecchina, *J. Catal.*, 2013, **308**, 319; (*c*) A. Budnyk, A. Damin, E. Groppo, A. Zecchina and S. Bordiga, *J. Catal*., 2015, **324**, 79.
14 M.-C. Daniel and D. Astruc, *Chem. Rev*., 2004, **104**, 293.
15 M. A. Fardad, *J. Mater. Sci*., 2000, **35**, 1835.
16 S. Cherkasova and A. Budnyk, *Inzhenernyi Vestnik Dona*, 2016, no. 3; URL: ivdon.ru/ru/magazine/archive/n3y2016/3750 (in Russian).
17 K. S. W. Sing, D. H. Everett, R. A. W. Haul, L. Moscou, R. A. Pierotti, J. Rouquerol and T. Siemieniewska, *Pure Appl. Chem*., 1985, **57**, 603.
18 W. P. Cai and L. D. Zhang, *J. Phys. Condens. Matter*, 1997, **9**, 7257.
19 C. Kan, W. Cai, Z. Li, G. Fu and L. Zhang, *Chem. Phys. Lett*., 2003, **382**, 318.
20 (*a*) T. Yao, Z. Sun, Y. Li, Z. Pan, H. Wei, Y. Xie, M. Nomura, Y. Niwa, W. Yan, Z. Wu, Y. Jiang, Q. Liu and S. Wei, *J. Am. Chem. Soc*., 2010, **132**, 7696; (*b*) B.-K. Pong, H. I. Elim, J.-X. Chong, W. Ji, B. L. Trout and J.-Y. Lee, *J. Phys. Chem. C*, 2007, **111**, 6281.
21 A. P. Budnyk, A. Damin, G. Agostini and A. Zecchina, *J. Phys. Chem. C*, 2010, **114**, 3857.
22 S. Link and M. A. El-Sayed, *Annu. Rev. Phys. Chem*., 2003, **54**, 331.

Received: 24th November 2016; Com. 16/5101